frontiers in Immunology

ORIGINAL RESEARCH
published: 06 December 2019
doi: 10.3389/fimmu.2019.02774

RETRACTED: Modeling Cardiac Dysfunction Following Traumatic Hemorrhage Injury: Impact on Myocardial Integrity

Johanna Wall[1†], Sriveena Naganathar[1†], Banjerd Praditsuktavorn[1], Oscar F. Bugg[1], Simon McArthur[2], Christoph Thiemermann[1,3], Jordi L. Tremoleda[1] and Karim Brohi[1]*

[1] Centre for Trauma Sciences, Neuroscience, Surgery and Trauma, Blizard Institute, Queen Mary University of London, London, United Kingdom, [2] Centre for Oral Immunobiology & Regenerative Medicine, Institute of Dentistry, Queen Mary University of London, London, United Kingdom, [3] Department of Translational Medicine and Therapeutics, William Harvey Research Institute, Queen Mary University of London, London, United Kingdom

OPEN ACCESS

Edited by:
Guochang Hu,
University of Illinois at Chicago,
United States

Reviewed by:
David N. Naumann,
University of Birmingham,
United Kingdom
Neil Herring,
University of Oxford, United Kingdom

***Correspondence:**
Jordi L. Tremoleda
j.lopez-tremoleda@qmul.ac.uk

[†]These authors have contributed equally to this work

Specialty section:
This article was submitted to Inflammation, a section of the journal Frontiers in Immunology

Received: 12 September 2019
Accepted: 12 November 2019
Published: 06 December 2019

Citation:
Wall J, Naganathar S, Praditsuktavorn B, Bugg OF, McArthur S, Thiemermann C, Tremoleda JL and Brohi K (2019) Modeling Cardiac Dysfunction Following Traumatic Hemorrhage Injury: Impact on Myocardial Integrity. Front. Immunol. 10:2774. doi: 10.3389/fimmu.2019.02774

Cardiac dysfunction (CD) importantly contributes to mortality in trauma patients, who survive their initial injuries following successful hemostatic resuscitation. This poor outcome has been correlated with elevated biomarkers of myocardial injury, but the pathophysiology triggering this CD remains unknown. We investigated the pathophysiology of acute CD after trauma using a mouse model of trauma hemorrhage shock (THS)-induced CD with echocardiographic guidance of fluid resuscitation, to assess the THS impact on myocardial integrity and function. Mice were subjected to trauma (soft tissue and bone fracture) and different degrees of hemorrhage severity (pressure controlled ~MABP < 35 mmHg or <65 mmHg) for 1 h, to characterize the acute impact on cardiac function. In a second study, mice were subjected to trauma and hemorrhage (MABP < 35 mmHg) for 1 h, then underwent two echocardiographic-guided resuscitations to baseline stroke volume at 60 and 120 min, and were monitored up to 180 min to study the longer impact of THS following resuscitation. Naïve and sham animals were used as controls. At 60 min post-THS injury, animals showed a lower cardiac output (CO) and stroke volume (SV) and an early rise of heart fatty acid-binding protein (H-FABP = 167 ± 38 ng/ml; 90% increase from shams, 3.54 ± 3.06 ng/ml), when subjected to severe hemorrhage and injury. Despite resuscitation, these animals maintained lower CO (6 ml/min vs. 23 ml/min), lower SV (10 μl vs. 46 μl; both ~75% decreased), and higher H-FABP (levels (340 ± 115 ng/ml vs. 10.3 ± 0.2 ng/ml; all THS vs. shams, $P < 0.001$) at 180 min post-THS injury. Histopathological and flow-cytometry analysis of the heart confirmed an influx of circulatory leukocytes, compared to non-injured hearts. Myocardial injury was supported by an increase of troponin I and h-FABP and the widespread ultrastructural disorganization of the morphology of sarcomeres and mitochondria. DNA fragmentation and chromatin condensation driven by leakage of apoptosis-inducing factor (AIF) may suggest a mitochondria-driven progressive cell death. THS modeling in the mouse results in cardiomyocyte damage and reduced

myocardial function, which mimics the cardiac dysfunction seen in trauma patients. This CD model may, therefore, provide further understanding to the mechanisms underlying CD and act as a tool for developing cardioprotective therapeutics to improve survival after injury.

Keywords: trauma, cardiac dysfunction, myocardial damage, haemorrhagic injury, murine models

INTRODUCTION

Trauma is a large and growing problem worldwide, accounting for 10.1% of the global burden of disease (1), with half of all trauma deaths being due to excessive bleeding and the subsequent severe shock (2, 3). New paradigms of hemostatic resuscitation to manage coagulopathy have led to large decreases in mortality worldwide (4, 5). With more patients surviving the initial bleeding episode, cardiac dysfunction is increasingly common and an important determinant of outcome. Over half of all critically injured trauma patients admitted to intensive care develop cardiovascular dysfunction within the first 48 h, of which 20% will die (6). Identifying these patients early in their care and rescuing them from this downward trajectory would have a dramatic impact on trauma mortality.

Cardiac dysfunction in trauma patients is initially difficult to recognize, as it develops within the context of hypovolemia and a widespread inflammatory response (7). Patients often initially show a normal cardiac response with a high cardiac output, but over a relatively short period they experience a dramatic fall in SV and CO, despite inotrope and vasopressor support. We have previously shown that trauma patients have elevated levels of biomarkers of myocardial damage within the first 2 h of injury, and this is associated with increased risks of adverse cardiac events and mortality (8, 9). Cardiac histopathology in non-survivors has shown multiple pathological identifiers of indirect or secondary cardiac injury (10, 11). The pathophysiology and mechanisms of secondary cardiac dysfunction are unknown, with most critical care studies limited to sepsis (12). There is some pre-clinical evidence for the development of cardiac injury and dysfunction arising as an indirect consequence of trauma and hemorrhage in pigs (13) and in rodents (14–16), suggesting a local cardiac inflammatory response as the main driver of cardiomyocyte structural and functional damage.

Our overall aim for this study was to investigate the pathophysiology of cardiac dysfunction after trauma by implementing a clinically relevant murine model of post trauma hemorrhage cardiac dysfunction. Specifically, our objectives were to: (1) determine the nature and extent of myocardial damage and cardiac dysfunction in an un-resuscitated model of trauma hemorrhage; (2) determine the progression of cardiac dysfunction over time in a resuscitated model of trauma hemorrhage; and (3) explore the inflammatory myocardial response and ultrastructural integrity, to elucidate possible mechanistic pathways for cardiomyocyte cell damage.

MATERIALS AND METHODS

Ethical Statement

All animal procedures were carried out under a Project License (PC5F29685) approved by the Animal Welfare and Ethical Review Body at Queen Mary University of London and the UK Home Office, in accordance with the EU Directive 2010/63/EU. All animal facilities and suppliers have been approved by the UK Home Office Licensing Authority and meet all current regulations and standards for the UK. A total of 98 mice were used for the work described in this study (details in **Supplementary Table 1**).

For this study we used $n = 6$–10 animals per group, to provide a valuable discriminatory power of 90% with a significance level of $\alpha = 0.05$ to detect up to 15–20% relative differences in primary outcomes (lactate levels, cardiac function, cardiac injury biomarkers). Experimental planning for data randomization and blinded data acquisition and analysis was carried out following the ARRIVE guidelines (17).

Animal Housing and Husbandry

Adult male C57Bl/6 mice (weight range 25–30 g; 9–11 weeks old) were obtained from Charles River Laboratories (Margate, UK). Health screens provided by the official vendor indicated that animals were free of known pathogens in accordance with FELASA guidelines for health monitoring of rodent colonies (18). Animals were housed in groups of 4–6 per individually ventilated cage (IVC; Allentown Europe, UK), in a 12 h light dark cycle (06:30–18:30 light; 18:30–06:30 dark), with controlled room temperature (21 ± 1°C) and relative humidity (40–60%). Animals were allocated to cages on arrival and remained in the same social group throughout the study, including a 7 day acclimatization phase prior to any study, with *ad libitum* access to standard diet and water.

Induction of Hemorrhagic Traumatic Injury

Animals were anesthetized (Isoflurane: 4–5% induction, 0.5–1.5% for maintenance in 0.8–1 lt/min 100% medical O_2). Anesthesia depth was controlled clinically and by hemodynamic monitoring (Mean Arterial Blood Pressure; MABP). Core temperature was maintained at 36± 1°C throughout the study with a homoeothermic blanket (Harvard Apparatus Ltd., UK) and heat lamps. All experiments were carried out under terminal anesthesia with no recovery, and all animals were humanely culled at the end of the experiment.

A 1 cm incision was made in the middle of the cervical skin and the left jugular vein was cannulated [polyethylene tubing pre-flushed with heparinized saline (25 IU/mL); Portex. Smith's

Medical Int. Ltd. Kent, UK] The right carotid artery was then cannulated in the same fashion and connected to a pressure transducer (Capto SP 844, AD Instruments, UK) attached to a PowerLab 8/30 (ML870, AD Instruments Ltd, Oxford, UK) to monitor MABP using the LabChart software (ADInstruments Ltd, UK). The neck incision was covered and regularly checked for evidence of line displacement and/or bleeding. If either of these developed, the animal was euthanized and removed from the study.

A 2 cm midline laparotomy was then performed, and the rectus muscle was crushed using forceps in a systematic fashion in each animal. The abdominal area was examined to exclude inadvertent iatrogenic injury and/or bleeding, and then the incision was closed using 5.0-prolene suture material (Ethicon, UK). Immediately thereafter, animals were subjected to a bilateral hind limb fracture. Fractures were performed using a closed, manual 3-point bending technique. Following 5 min' stabilization after traumatic injury, a "baseline" MABP was recorded. Then, a pressure-controlled hemorrhage via the carotid cannula was induced to achieve a target MABP of 30–40 mmHg to reach a traumatic hemorrhagic shock state (THS). Animals underwent a 60 min observation period, during which the target blood pressure (30–40 mmHg) was maintained with removal of blood as required via the carotid cannula. Shed blood was kept warm in a heparinized 1 mL syringe (25 IU/mL), which was occasionally agitated to prevent thrombus formation. In-dwelling vascular catheters were intermittently flushed with small volumes of heparinized saline and wound sites checked for signs of hemorrhage. All volumes of heparinized saline were taken into account when recording volumes of shed and reinfused blood.

Sham controls underwent cannulation of the carotid artery for invasive MABP monitoring only, without trauma, hemorrhage or fluid resuscitation.

Echocardiography of the left ventricle (LV) was performed at baseline (prior to any traumatic hemorrhagic intervention), and at defined time-points after injury to assess the impact of THS injury at 60 (T60), 120 (T120), and 180 (T180) min post THS, using the Vevo 770 high-resolution system (Visualsonics Inc. Toronto, Canada). M-mode short axis measurements were used to calculate stroke volume (SV), left ventricular end-diastolic volume (LVEDV), and cardiac output (CO). Measurements were carried out in triplicate.

The acute impact of THS in cardiac function was studied in animals subjected to sham, trauma only, THS to 60–70 mmHg MABP or THS to 30–40 mmHg MABP procedures ($n = 6$/group) following 1 h post-intervention, without any resuscitation. At 60 min post THS (T60), cardiac function and shock status were assessed and animals were culled via terminal exsanguination and blood samples processed for further analysis (**Figure 1A**).

To investigate the CD associated with THS, the THS model with a 30–40 mmHg MABP was extended up to 3 h through 2 resuscitation phases at T60 and T120 (THS and sham, $n = 10$/group) and terminated at T180. Echocardiography was carried out at T60, T120, and T180 to assess cardiac function and also to guide the resuscitation volume requirements to restore the SV to baseline levels during each resuscitation at T60 and T120 (**Figure 2A**).

For the first resuscitation (RESUS 1 at T60), the whole shed blood was transfused as a bolus over 5 min *via* the jugular catheter, and boluses of warmed Hartmann's solution (Vetivex11. Dechra Veterinary Products, Shrewsbury, UK) were then administered to reach SV baseline. In the second resuscitation phase (RESUS 2 at T120), a bolus of Hartmann's alone was administered over 5–10 min. At each resuscitation, animals received volume resuscitation to restore left ventricular stroke volume to baseline. During the second resuscitation, if the target SV was not reached and yet there was no incremental response to further fluid boluses (and in the confirmed absence of bleeding from wound sites), this was deemed to represent the completion of the resuscitation phase. All studies were terminated at T180, through controlled exsanguination via carotid line and confirmation of death via HR and MABP.

At the end of the experiment, sham animals were culled *via* terminal exsanguination and blood samples and tissue taken.

Assessment of Shock Status

MAPB and heart rate were measured throughout hemorrhage and resuscitation. Blood lactate was measured and used as an index of shock and tissue perfusion. Arterial lactate concentrations (mmol/L) were assessed using the Accutrend Lactate monitor (Roche, Mannheim, Germany). Echocardiography measured at T60 and T120 before and after resuscitation, and at T180 was carried out to assess cardiac function (left ventricle SV). Hematocrit (Hct; %) and hemoglobin (Hb; g/dL) were measured with a ProCyte Dx Hematology Analyzer (IDEXX Europe B.V, Hoofddorp, The Netherlands).

Terminal Blood Sampling and Tissue Storage

Terminal exsanguination was performed via the carotid catheter only and processed for serum separation (Z-Gel microtube, Starstedt. Westphalia, Germany). Serum samples were stored at −80°C. The hearts were removed immediately after the end of the experiment and processed accordingly to further test specifics.

Cardiac Biomarker Assessment

Serum heart fatty acid-binding protein (H-FABP) levels were assayed using commercially available mouse specific enzyme-linked immunosorbent assay (ELISA Cat. No. HFABP-1) kit (supplied by Life Diagnostics Inc., West Chester, PA, USA.). ELISAs were performed in accordance with the manufacturer's instructions. Standard curves for all ELISAs were plotted and dilution-corrected sample concentrations were interpolated from the standard curve.

Immunohistochemistry Analysis

At 3 h THS, a subset of animal ($n = 3$ naïve, $n = 5$ THS) were terminally anesthetized and cardiac tissue was immediately fixated (10% NBF). Naïve animals were housed together under the same conditions but did not have any surgical intervention, trauma, hemorrhage or fluid resuscitation. Cardiac tissue was paraffin-fixed for histology and immunohistochemistry (IHC).

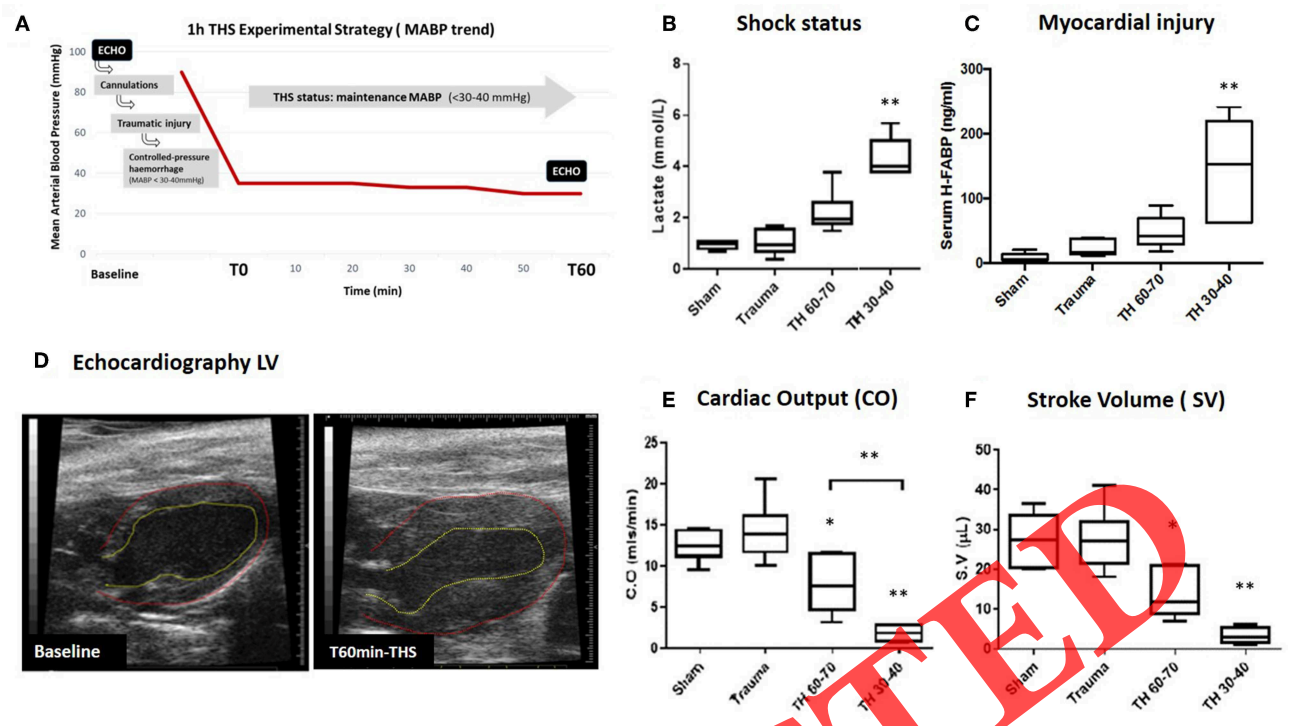

FIGURE 1 | Characterization of the shock status and cardiac dysfunction at 60 min post traumatic hemorrhagic shock injury (1 h post-THS). **(A)** Modeling strategy describing the experimental set up with vessel cannulations, traumatic soft and hard tissue injury and pressure-controlled hemorrhage. **(B)** Median values, interquartile range and range of arterial blood lactate levels at 60 min post-THS between the experimental groups (S, sham with only vessel cannulation only; T, Traumatic injury alone; TH 60–70, THS with 60–70 mmHg; MABP and TH 30–40, THS with 30–40 mmHg MABP). $^{**}P < 0.001$ between TH 30–40 and S, T, and TH 60–70. **(C)** Serum H-FABP levels as a myocardial injury biomarker at 60 min post-THS between the S, T, and THS 60–70 and 30–40 mmHg groups, showing a significant difference in the THS-30–40 group vs. the others ($^{**}P < 0.001$). **(D)** Representative echocardiographic images across the longitudinal heart axis showing the collapsed LV in THS animals at 60 min post-injury, in comparison with baseline non-no injured heart; yellow line depicts the endocardium; red line depicts epicardium. **(E)** Cardiac outcome (CO; ml/min) at 60 min post-injury, showing the impact of pre-load effects on the THS 60–70 and the THS 30–40 groups compared to S and T groups ($^{*}P < 0.05$, $^{**}P < 0.001$ between groups; $^{**}P < 0.01$ TH 60–70 vs. TH 30–40). **(F)** Stroke volume (SV; µL) at 60 min post-injury, showing the impact of pre-load effects on the THS 60–70 and the THS 30–40 groups ($^{*}P < 0.05$, $^{**}P < 0.001$ between groups).

Sections (7 µm) were deparaffinized and hydrated through xylene and ethanol baths. Sections were subjected to antigen retrieval (10 mM of citrate buffer, pH 6.0, 10 min in microwave) and then cooled at room temperature. Tissue was permeabilized with 10% Triton-X in PBS for 15 min and then blocked with 10% goat or donkey serum, 1% bovine serum albumin (BSA) in PBS for an hour, at room temperature (RT). The following primary antibodies diluted in blocking solution were used (overnight incubation in a humid chamber at 4°C): goat anti-ionized calcium binding adaptor molecule 1 (Iba-1; for macrophages and monocytes 1:500; Wako Chemicals USA, Inc., Richmond, VA; Cat#ab109497), rat anti-Lymphocyte antigen 6 complex, locus G (Ly6G-clone 1A8; for neutrophils 1:200; BioLegend, London, IK; Cat# 127602); rabbit anti-mouse cleaved caspase-8 1:200 (Asp387; Cell Signaling Tec.; Cat#8592); rabbit anti-mouse MTCO2 (1:125; Abcam plc, Cambridge, UK; Cat#ab110258); or rabbit polyclonal anti-AIF (1:100; Abcam, UK; Cat#ab2086). The secondary antibodies were donkey anti-goat IgG 568, goat anti-rat 594 IgG, goat anti-rabbit IgG 488 or goat anti-mouse IgG 594 (Molecular Probes, Leiden, the Netherlands; 1:400 in PBS). Sudan black (0.3% w/v in 70% ethanol) was used to reduce autofluorescence and Hoescht 33342 stain (Sigma-Aldrich, Gillingham UK; 1 µg/ml of PBS) was used to visualize nuclei. Slides were mounted and cover-slipped using Vectashield mounting medium (H-1000, Vector Laboratories, Burlingame, CA).

For calculations, 2 slides per animal with at least 18 fields were captured across the short-axis LV myocardium stained section. Images were viewed (x400) and photographed using a Zeiss Axioskop 2 microscope (Carl Zeiss, Jena, Germany) with a Hamamatsu camera (C4742-95; Hamamatsu Photonics K.K., Hamamatsu, Japan). Analysis was done using the ImageJ analysis software for counting the number of positively stained cells. Total nuclei count was measured to normalize percentage of positive stained cells across fields. All imaging acquisition and analysis were carried out blinded to the experimental interventions, and data were only allocated to the specific experimental group at the end of the analysis.

Flow Cytometry Full Heart Analysis

At 3 h post-study, a subset of animals ($n = 6$ naïve, $n = 5$ sham-subjected to vessel cannulation and terminal anesthesia only, n

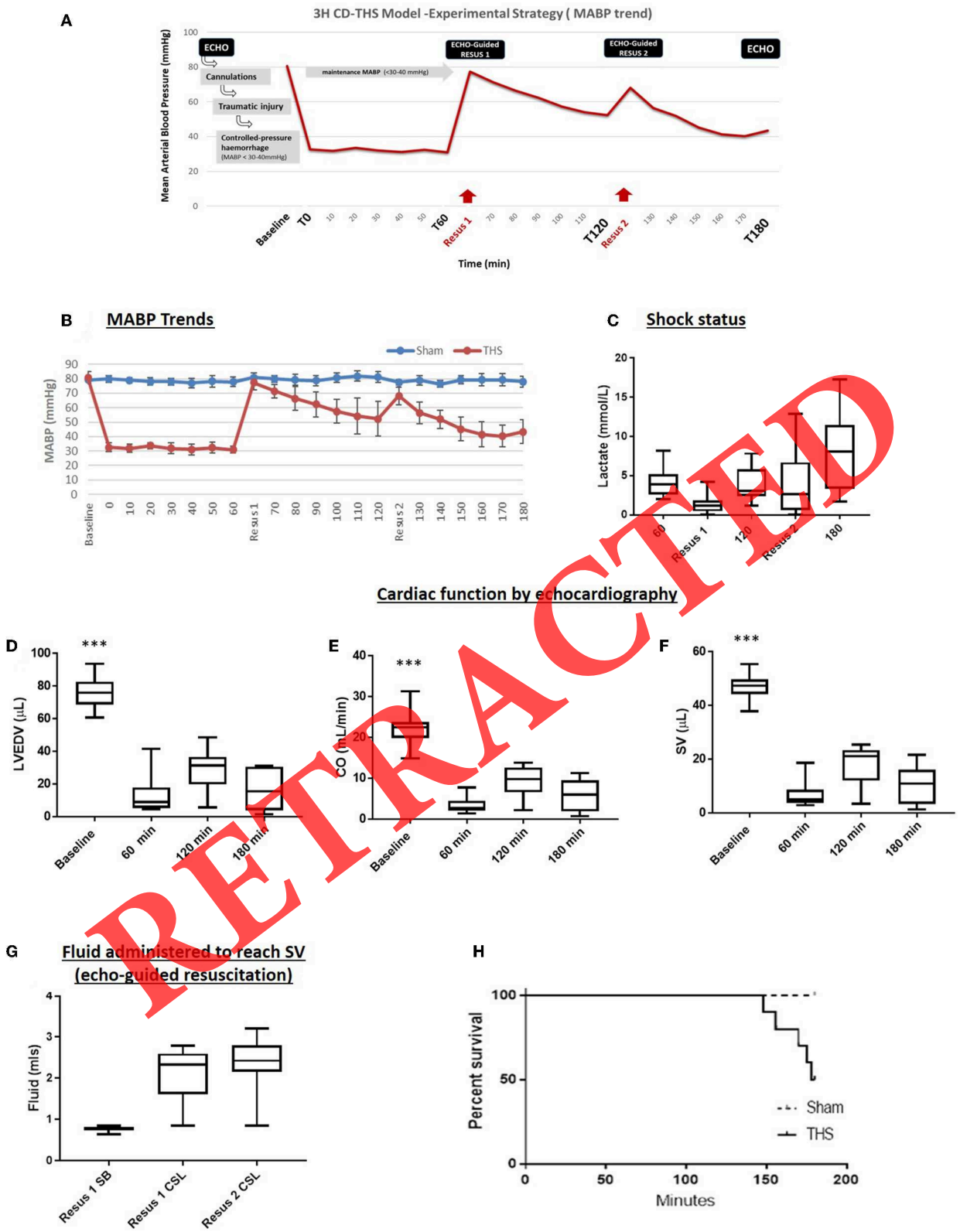

FIGURE 2 | Characterization of the 3 h THS cardiac dysfunction (CD) model. **(A)** Modeling strategy: mice subjected to trauma hemorrhage are held at a MAP of 30–40 mmHg for an hour and then resuscitated with shed blood & crystalloid (Resus1) to their original stroke volume (SV). Mice are then left for a further hour and

(Continued)

FIGURE 2 | resuscitated again (Resus 2) and then left to complete a 3 h experiment. Animals undergo two echocardiographic-guided resuscitations at 60 and 120 min to baseline SV. **(B)** Progressive decrease of MABP despite pre-load resuscitation fluids. **(C)** Serum lactate levels increase steadily after the 1st resus (3.93 ± 0.93 mmol/L) to T180 post-THS (7.9 ± 5.19 mmoL). **(D)** Left ventricular end-diastolic volume (LVEDV) does not regain baseline levels despite resuscitation pre-loads (Baseline: 76.17 ± 10.15 vs. 180 min 16.40 ± 12.98 at T180 post-THS; ***$P < 0.0001$ *vs.* all other groups, one-way ANOVA). **(E)** Cardiac Output (CO; ml/min; ***$P < 0.0001$ *vs.* all other groups, one-way ANOVA) and **(F)** SV (μL) indicate the progressive loss of LV function despite pre-load resuscitation (***$P < 0.0001$ *vs.* all other groups, one-way ANOVA). This is observed already following the 1st resus after T60 THS insult, despite temporary increases in CO and SV immediately following resuscitations (at T60 and T120; see **Supplementary Table 4**). **(G)** Following the initial dosing of shed blood (SB) during the 1st resus at T 60 min, the crystalloid fluid require to reach baseline SV is steadily increased during the 1st and 2nd resuscitation (THS60 min and THs 120 min, respectively). **(H)** Impact of CD in the median survival, with 50% decrease survival at THS 180 min.

= 5 THS) were intracardially perfused with heparinized saline under terminal anesthesia. The hearts were then immediately isolated, cut into 1 mm^3 pieces and dissociated by incubation with papain (Merck, UK) and DNAse I (ThermoFisher Scientific, UK) for 30 min at 37°C. Following lysis of residual red blood cells (RBC Lysis Buffer, Biolegend, UK), cell suspensions were incubated with CD16/CD32-block (Biolegend, UK) for 30 min at 4°C, followed by incubation for 30 min at 4°C with PE-conjugated anti-CD45 to define immune cell populations, and FITC-conjugated anti-Ly6C/G (clone RB6-8C5) and APC-conjugated anti-F4/80 (all ThermoFisher Scientific, UK) to differentiate neutrophils (F4/80Neg, Ly6C/GHi) from pro-inflammatory (F4/80Pos, Ly6C/GInt) and anti-inflammatory (F4/80Pos, Ly6C/GLow) monocytes/macrophages (19, 20). Cells were then analyzed by flow cytometry using a BD FACSCanto II instrument (BD Biosciences) and FlowJo 8.8.1 software (TreeStar Inc., FL, USA). In all cases, 20,000 singlet CD45Pos events were analyzed per sample; positive staining was defined by inclusion of fluorescence-minus-one controls for all antigens.

Transmission Electron Microscopy (TEM)

TEM was used to study micro-structural changes associated to specific cell injury and death in the cardiomyocyte following THS. In a subset cohort of THS and sham animals from the 3 h studies, the animals were humanely killed by overdose of anesthesia and the heart tissue immediately dissected, cut into smaller tissue specimen (~1 mm^3), and fixed in 2% glutaraldehyde. Fixed tissue was washed three times in cacodylate buffer 0.1 M pH 7.4 and then incubated in 1% osmium tetroxide in ddH2O for 2 h at 4°C. After 3 washes in ddH_2O, specimens were dehydrated (progressive incubation from 25 to 100% acetone) following by impregnation in an increasing concentration of the epoxy resin Araldite 502 (from 25 to 100% of araldite in acetone) used as the embedding medium for TEM. Samples were stored in fresh araldite for up to 72 h and then stored at 60°C for 48 h until the block was hard.

Protein Expression in the Heart

Western blotting (WB) was used to study biochemical changes associated to cardiomyocyte injury (troponin I, H-FABP) and cell death pathways (Caspase 8 and Apoptosis Inducing Factor-AIF) following THS. Tissue from THS ($n = 6$) and sham ($n = 6$) animals was used. At 3 h post-study, animals were deeply anesthetized and heart tissue was immediately dissected, weighted and immersed in RIPA buffer [0.1 g/1 ml w/v; 50 mM TrisHCl (pH 7.4), 150 mM NaCl, 1% Triton X-100, 0.5% sodium deoxylcholate, 0.1 % SDS, 1 mM EDTA, 10 mM NaF in ddH2O] with a cocktail of protease inhibitor and phosphatase inhibitor tablets (Pierce™ Protease and Phosphatase Inhibitor Mini Tablets Cat no. 88668, Sigma-Aldrich, UK). The tissue was minced in RIPA on a cooling slide on dry ice and mash in Dounce homogenizer. The sample was then sonicated (50 pulses in rounds of 10 s with 10 s rest). Samples were spun (@13,000 rpm in cooling centrifuge for 20 min) and the supernatant protein sample was collected. Protein concentrations were determined by Bradford assay. Equal amounts of protein sample were mixed with NuPAGE® MOPS SDS Running Buffer. 20X)-NP0001 was made up and a tank filled. Bolt™ 4–12%, 10-well NW04122BOX) Bis-Tris Plus Gel was inserted into the tank; 10 μl of samples were loaded with protein ladder (RPN800E-GE health care) into 10 well NuPage Bis-Tris Mini gel. Optical density was determine using ImageJ software (NIH). A cardiac tissue specific, mouse monoclonal troponin I antibody (Ab10231, Abcam, UK; 24 kDa) was used for the labeling of troponin. Caspase-8 (rabbit monoclonal anti-cleaved caspase 8; 8592S; Cell Signaling, UK; 41 kDa) expression was used as a marker of activation of death receptor initiated cell death pathway. AIF (rabbit polyclonal anti-AIF; Ab2086; Abcam, UK; 67 kDa) expression and location was assessed by WB analysis, with the tissue homogenates being processed for differential centrifugation to assess the sub-cellular compartmentation, removing the large organelles nuclei, cellular debris and intact cells, and allowing for selective extraction of the cytosol and mitochondria using Cytosol and Mitochondrial Extraction Buffer Mix containing DTT and Protease Inhibitors. MTCO2 (Anti-MTCO2; Ab198286; Abcam, UK; 1/150–25 kDa) and GAPDH (Anti-GAPDH antibody; Ab8245; Abcam, UK) were used as a mitochondrial and cytosol markers, respectively.

Statistical Analysis

Lactate levels (mmol/L), MABP measurements (mmHg), resuscitation fluids (ml), echocardiographic LV data (CO = ml/min; SV = μl; LDEDV = μl), % of inflammatory cells (neutrophils/monocytes/macrophages) and H-FABP serums levels = ng/ml) were expressed using mean values, with standard deviation (SD). Statistical analysis was performed using GraphPad Prism 8 (GraphPad Software, San Diego, USA). Normally distributed data was analyzed using Student's two-tailed *t*-test or one-way ANOVA, followed by Tukey's multiple comparison test. Non-normally distributed data was analyzed with Kruskall-Wallis and Mann-Whitney U test analysis. $P < 0.05$ was taken to represent significance. All analysis was performed blinded to the experimental interventions (Further details in **Supplementary Table 2**).

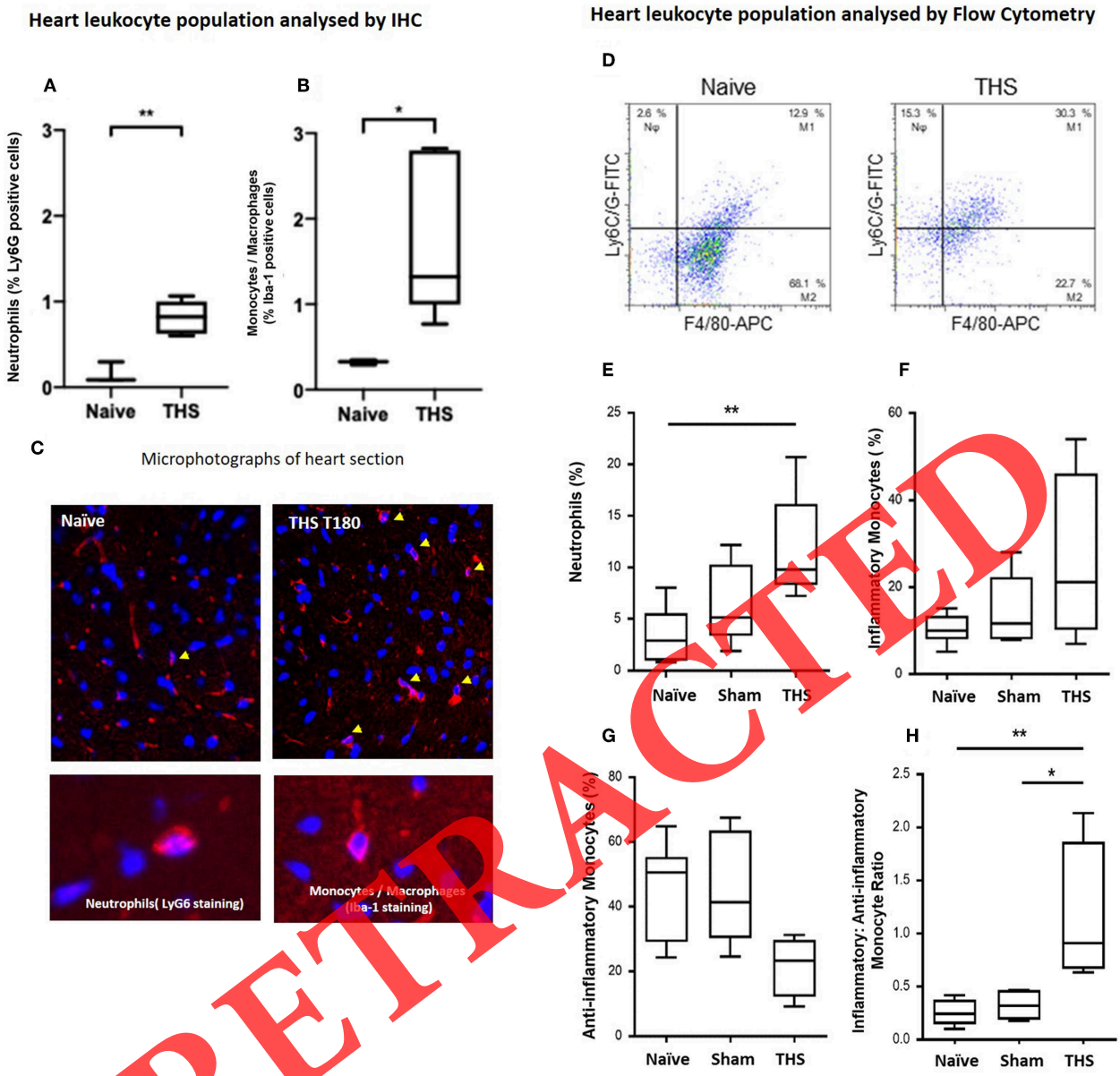

FIGURE 3 | Characterization of acute cardiac inflammation response in the Trauma Hemorrhage induced CD murine model (THS). Immunohistochemistry (IHC) myocardial analysis shows **(A)** a significant increase in neutrophils (% Ly6G cells) and **(B)** Monocytes/Macrophages (% Iba-1 cells) in the THS model (T180 min) compared to naïve (**$p < 0.001$, *$p = 0.02$; two-tailed unpaired *t*-test). Data is presented as means ± SD. **(C)** Representative IHC microphotographs in heart section in a THA and naïve animal (x400) and zoom insets of the LY6G and Iba-1 staining (red) for the neutrophils and monocyte/macrophage, respectively, with the nuclei Hoechst staining (blue) in a THS model. **(D–H)** Flow cytometry assessment of heart-infiltrating leukocytes. **(D)** Representative forward scatter/side scatter profile and a live cell gate. Following a CD45/side scatter plot to obtain the CD45+ leukocyte2, Ly6G Hi, or low expression with F4/80 plots was used to derived percentages of pro-inflammatory monocytes (Ly6GHi, F4/80+: M1 phenotype) and anti-inflammatory monocytes/macrophages (Ly6GLow, F4/80+: M2 phenotype). The heart from THS animals showed a significant increase in the M1:M2 phenotype ratio, compared to the naïve animals. **(E)** A significant presence of neutrophils (% Ly6G+ F4/80- cells) and a high ratio of inflammatory monocytes (**F–H**; Higher ratio of Ly6GHi, F4/80+ inflammatory monocytes vs. F4/80+: M2 anti-inflammatory macrophages/monocytes; **$p < 0.001$, *$p = 0.02$; one-way ANOVA with *post-hoc* analysis). Data all presented as means ± SD.

RESULTS

Myocardial Injury After Trauma and Hemorrhage

The trauma hemorrhage model demonstrated progressive myocardial damage and cardiac dysfunction following an hour of trauma and hemorrhage without resuscitation (**Figure 1**). We examined cardiac effects of trauma alone, trauma and hemorrhage to target MABP of 60–70 mmHg (THS 60–70); and to a target an MABP of 30–40 mmHg (THS 30–40), achieving different depths of shock severity (**Figure 1A**; **Supplementary Table 3**) Myocardial damage, as measured by

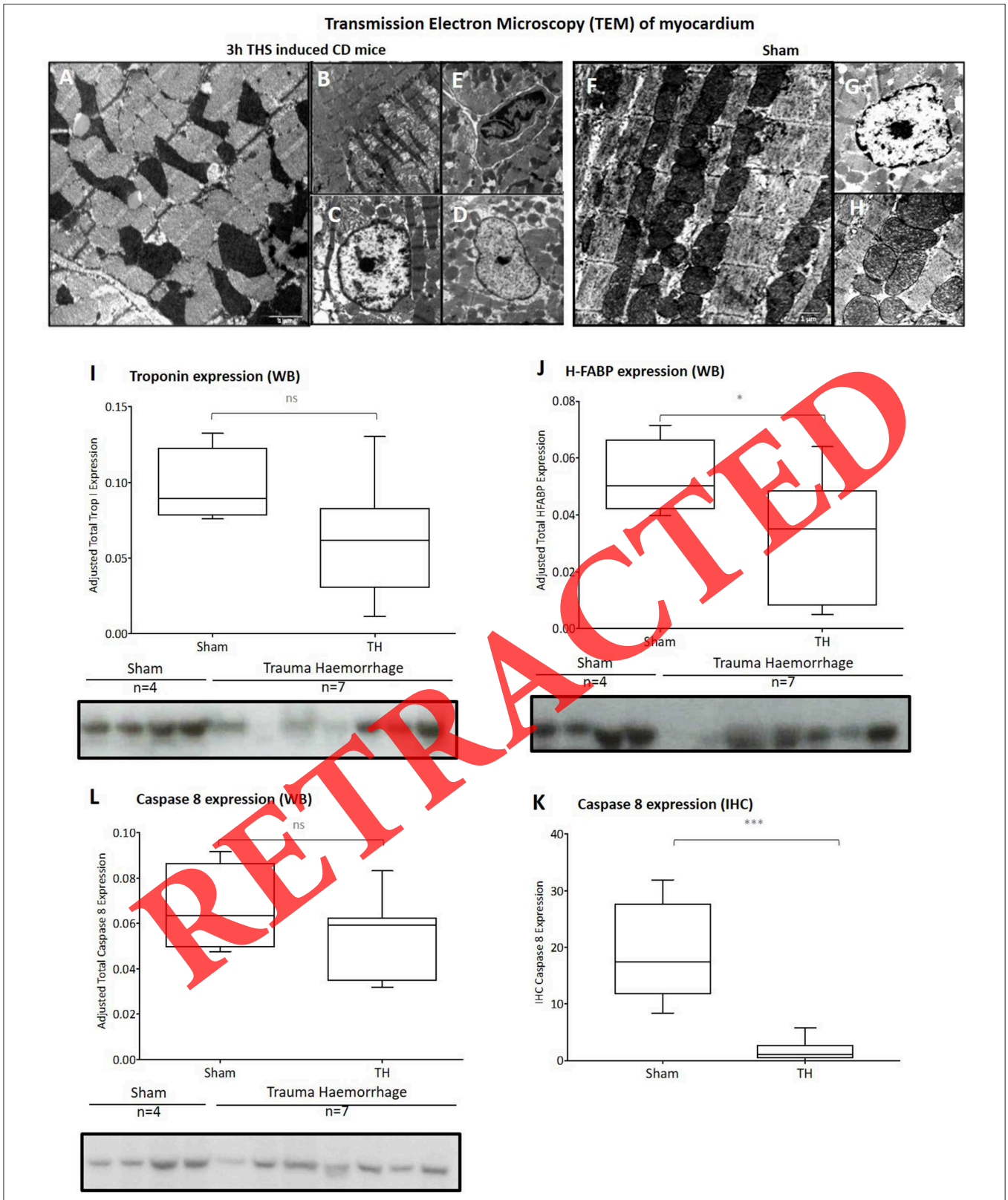

FIGURE 4 | Myocardial injury in the trauma hemorrhage induced CD murine model. TEM shows severe myocardial injury in the heart of THS mice, with interstitial oedema, widespread disorganization of the myoc ardium with relaxation of the sarcomere and poorly circumscribed mitochondria distributed in a disorderly fashion

(Continued)

FIGURE 4 | (A). Significant amounts of mitochondrial oedema **(B)** Nuclei shows margination of chromatin, rarefaction of the nucleoplasm **(C)** and glycogen depletion **(D)**; and some cardiomyocytes dead cells with margination of chromatin **(E)**. TEM of sham mice heart tissue shows a well-organized myofibrils, with mitochondria evenly organized along the cristae sarcomere **(F)** with intact nucleus **(G)** and mitochondria **(H)**. WB analysis of Troponin-I (cTnI) **(I)** and H-FABP **(J)** expression shows elevated levels in the myocardium of THS mice ($p = 0.06$ NS; $^{*}p = 0.04$, respectively; two-tailed unpaired *t*-test; means ± SD). **(K,L)** Low caspase 8 expression is observed in heart of THS mice (IHC $^{***}p < 0.0001$; WB $p > 0.05$ compared to sham animals).

serum H-FABP concentrations, increased with increasing model severity, and were significantly elevated for the most severe THS group (THS 30–40 = 166.69 ± 38.64 ng/ml), compared to sham, trauma only and 60–70 mmHg THS group ($p < 0.01$, **Figure 1C**). At end-experiment, stroke volume and cardiac output were significantly decreased from baseline in all groups (**Figures 1D–F**). In the THS 30–40 group, with over 30% blood loss, cardiac output was 87% lower than baseline (**Figure 1E**) at 1 h post trauma compared to sham and trauma-only groups ($p < 0.001$, **Figure 1E**).

Cardiac Dysfunction Following Myocardial Damage

In order to determine the functional effects of myocardial damage, we extended our TH 30–40 mmHg model for 3 h to include two resuscitation phases at 60 and 120 min post-hemorrhage (**Figures 2A,B**). Shock severity worsened over time despite the two resuscitation steps (**Figures 2B,C**), with serum lactate reaching a median of 7.9 ± 5.2 mmol/L at 180 min (from 1.4 ± 0.37 mmol/l at baseline $p = 0.004$, **Supplementary Table 4**). MABP increased immediately after resuscitation, but then progressively declined, despite transient increases with volume resuscitation. End-experiment MABP was 44% lower than post Resus-1 levels (43.3 ± 8 vs. 77.4 ± 5 mmHg **Figure 2B**; **Supplementary Table 4**). Hb concentration and Hct were not significantly different between the THS group and sham, at 3 h (Hb 14.5 ± 1.6 vs. 13.2 ± 1.4 and Hct 47.5 ± 8.7 vs. 43.1 ± 5.4, in sham and THS groups, respectively, **Supplementary Figure 1**).

On functional echocardiographic assessment, volume resuscitation to normalize stroke volume did not maintain LVEDV, stroke volume, or cardiac output. Mean LVEDV was only 23% of baseline at end-experiment (16.40 μl vs. 76.17 μl; $p < 0.0001$); stroke volume was 22% of baseline (10.5 μl vs. 47.1 μl, $p < 0.0001$) and total cardiac output was 30% from baseline (5.8 μl vs. 22.4 μl, $p < 0.0001$, **Figures 2D–G**; **Supplementary Table 4**). In line with these findings, H-FABP concentrations continued to increase from T60 min post-THS, rising to a mean of 340 ng/ml at end-experiment compared to 116.7 ng/ml at T60 ($p = 0.003$) and 10.3 ng/ml compared to sham animals at end-experiment, $p < 0.001$, **Supplementary Table 4**). Despite resuscitation, 50% of animals had died by 3 h post-hemorrhage (**Figure 2H**).

Myocardial Inflammation and Structural Damaged Following THS Impacts on Cardiomyocyte Survival

From our *in situ* IHC-analysis in the myocardium, a significantly higher % of neutrophils (Ly6G stained cells) was identified in the heart of the THS group compared to naïve animals (0.15 ± 0.07 vs. 0.8 ± 0.1% of positive LyG66G cells, respectively; $P = 0.02$, **Figures 3A,C**); a high presence of macrophages and monocytes were also identified in the THS group (1.7 ± 0.01 vs. 0.3 ± 0.01% positive Iba-1 cells in THS vs. naïve, respectively; $P = 0.001$, **Figures 3B,C**).

From the flow cytometry analysis carried out following *ex vivo* heart cells disaggregation, a significantly higher number of neutrophils were identified in THS group compared to naïve non-injured animals (11.7 ± 5.2 vs. 3.4 ± 2.7% F4/80Neg, Ly6C/GHi cells; one way ANOVA with Tukey's multiple Comparison $P = 0.01$) (**Figures 3D,E**). Sham animals did not differ from naïve or THS (6.4 ± 3.9% F4/80Neg, Ly6C/GHi cells). When investigating monocyte cell population, we identified a statistically higher ratio of pro-inflammatory (F4/80Pos, Ly6C/GInt) vs. anti-inflammatory (F4/80Pos, Ly6C/GLow) monocytes in the THS group compared to the naïve and sham animals (1.14 ± 0.8 for THS group vs. 0.25 ± 0.1 for naïve group and 0.32 ± 0.1 for sham group; $P = 0.006$ and $P = 0.01$, respectively, **Figures 3F–H**). There was also a trend to shift the presence of pro vs. anti-inflammatory monocytes in the hearts of THS animals, compared to that for the naïve and sham groups; but these data did not reach the threshold for statistical significance (**Figures 3F,G**).

TEM analysis demonstrated significant morphological changes within the myocardium, with interstitial oedema and widespread disorganization of the cardiac myofibrillar ultrastructure, and a relaxation of the sarcomere in the cardiomyocytes (**Figure 4A**). We identified the presence of poorly circumscribed mitochondria distributed in a disorderly fashion across cardiac muscle fibers, with significant structural changes. In THS animals, 33% of the mitochondria contained amorphous dense bodies, in comparison to 23% in the sham animals ($p = 0.006$). Mitochondrial swelling, with loss of electron dense material from the matrix and breakdown of the cristae and vacuolation, was also observed in THS animals (**Figure 4B**). The nuclei of this THS group also exhibited signs of irreversible structural changes, such as margination of chromatin, associated with surrounding oedema, chromatin condensation, and rarefaction of the nucleoplasm, where there is loss of the chromatin (**Figures 4C–E**), compare to sham animals (**Figures 4F–H**). Most of these lesions are consistent with presence of myocardial ischemia injury the THS hearts (**Figure 4**).

Myocardial damaged was confirmed by the reduced levels of H-FABP in the myocardium of the THS hearts ($p = 0.06$ NS; $^{*}p = 0.04$, respectively; two-tailed unpaired *t*-test; means ± SD), indicating the loss /release of these proteins, attributable to myocardial injury (**Figures 4I,J**).

A significant decrease in caspase 8 expression in THS was seen on IHC (**Figure 4K**) is suggestive that the cardiomyocte

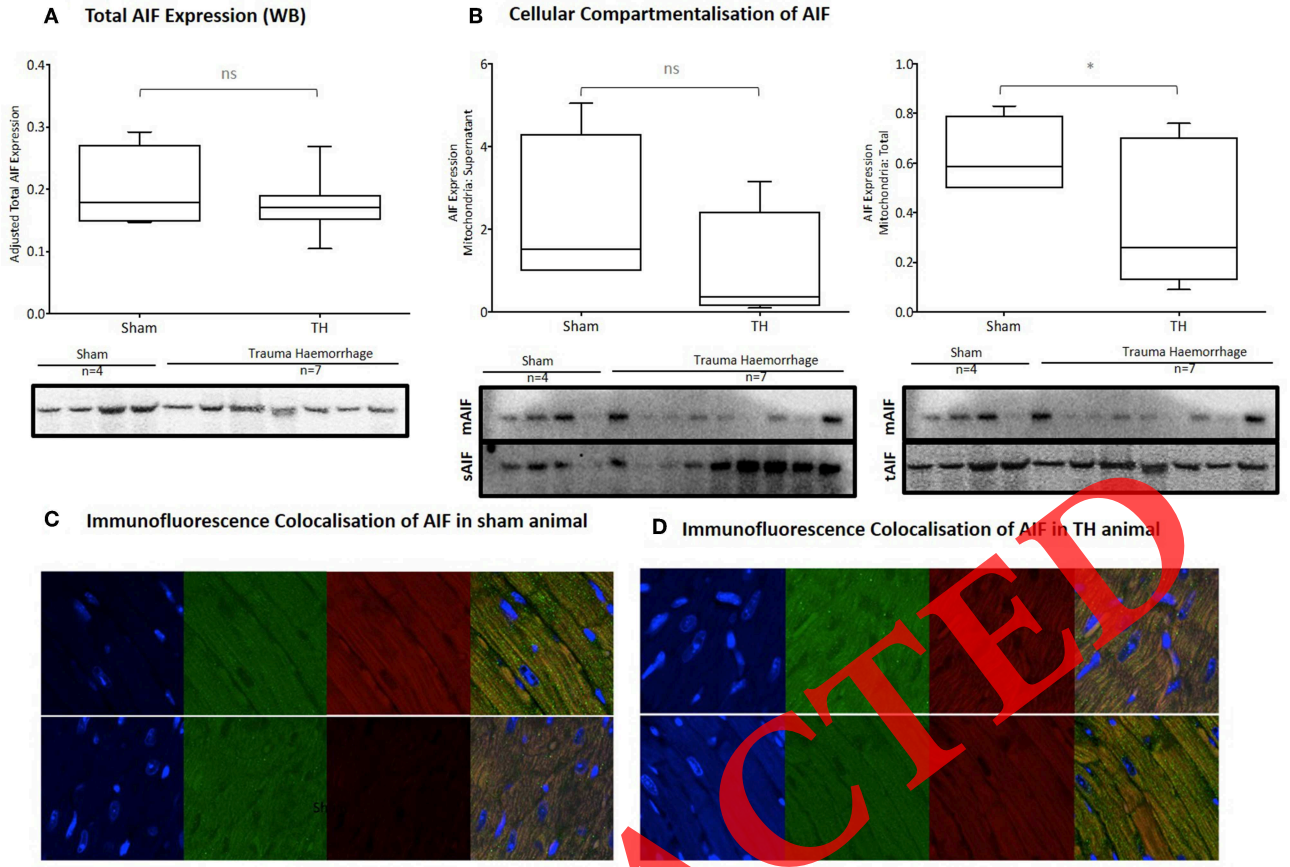

FIGURE 5 | AIF localization in the trauma hemorrhage induced CD murine model. **(A)** AIF expression as demonstrated by western blot analysis. The total AIF expression is similar in the Sham and THS models (0.20 vs. 0.17, respectively). **(B)** Cellular compartmentalization of AIF as demonstrated by WB analysis. A higher proportion of AIF is found outside the mitochondria in the THS models. The mean ratio of mitochondrial AIF (mAIF) to supernatant AIF (sAIF) is 1.5 in sham compared to 0.4 in THS group, $p = 0.16$. When comparing total AIF which includes the nucleus, a lower proportion is still found in the mitochondria. Ratio of mitochondrial AIF (mAIF) to total AIF (tAIF) in sham group is 0.6 compared to 0.3 in THS animals, $^{*}p = 0.04$. This is suggestive of its translocation of the AIF out of the mitochondrion, potentially to the nucleus, triggering initiation of cells death. IHC sections from TH animals, DAPI (blue), AIF (green), MTCO2 (red), and combined images. In the combined images, localization of AIF in the nucleus can be seen in the THS **(D)** which in absent in the sham animals **(C)**.

damage seen is not dependent upon death receptor initiated or protease dependent apoptosis. The difference in caspase 8 on WB although downward trending was not statistically significant (**Figure 4L**). The total AIF expression was similar between Sham and THS models (0.20 vs. 0.17 respectively, NS, **Figure 5A**), but a compartmentalization of AIF outside the mitochondria was observed in the TH models. The decrease in the mitochondrial AIF in comparison to cytosolic AIF in the THS hearts (mitochondria vs. total cell $P = 0.04$ and mitochondria vs. supernatant/cytosol $P = 0.04$, **Figure 5B**) suggests a leakage of the mitochondrial AIF into the cytosol, with the potential activation of a mitochondrial driven cell death pathway (**Figures 5A–D**).

DISCUSSION

Our study confirms that the preclinical modeling approach that we have developed physiologically and biochemically mirrors the cardiac dysfunction seen in bleeding trauma patients. Traumatic injury and controlled hemorrhage induced significant acute cardiac damage despite subsequent echocardiography-guided volume resuscitation. These changes were associated with demonstrable myocardial cell death and inflammation leading to reduced survival.

In our unresuscitated model, we identified cardiac functional changes and myocardial damage with comparable elevations in the cardiomyocyte damage molecule H-FABP (21) to those reported in clinical studies (8, 22). The associated functional decreases in cardiac output were at least in part related to the loss of stroke volume. However, our resuscitated model, with confirmed restoration of volume preload, demonstrated a persistent and progressive loss of cardiac function associated with increasing myocardial injury indicated by further elevations in H-FABP. Catecholamine release with increased inotropy will undoubtedly compensate for some degree of cardiomyocyte loss. However in our model, volume resuscitation to baseline LVEDV was not able to restore cardiac function to pre-shock levels. This resultant cardiac dysfunction is increasingly recognized as a key

determinant of critical care utilization and survival in trauma patients (10, 23, 24).

Cardiac dysfunction is well-known in sepsis (12, 25), but the etiology of trauma induced myocardial injury likely has different underlying pathophysiology (1–16, 26). We observed an acute cardiac inflammatory response, with an increase in monocytes/macrophages and neutrophils infiltration in the heart is identified following THS injury. This may be driven by the systemic inflammatory response to trauma (15, 26), or may be a direct response of the immune system to cardiomyocyte cell death. The acute recruitment of monocytes and neutrophils from circulation into the myocardium has also been reported in cardiac stress ischemic conditions (27). The persistence of this myocardial inflammation response may lead to further endogenous cytokine production and leukocyte recruitment and infiltration, increasing oxidative stress, cell damage and cardiac dysfunction (28).

We observed severe cardiomyocyte ultrastructural and organelle dysfunctional damage by 3 h post trauma, with myofibrillary disarray, relaxation of sarcomeric proteins, mitochondrial vacuole formation, membrane disruption and chromatin features consistent with irreversible damage. Such cellular stress features, augurs of cell death, have been described in rodent cardiomyocytes following ischemia-reperfusion (29). Furthermore, the increased translocation of mitochondrial AIF into the cytosol, and then into the nucleus, confirms the activation of cell death pathways associated with cell death. This presence of AIF leakage in addition to the reduced expression of caspase 8, may indicate the involvement of the alternate cell death pathway of necroptosis as a principle mode of cardiomyocyte cell death in trauma (30, 31). Many alarmins released following trauma (ATP, DNA, histones, HMGB-1, HSP70) have been associated with necroptosis signaling (32), and such necroptosis has already been identified as central to other sterile inflammation conditions such as acute pancreatitis (33) and organ injury (34). Our data raises the possibility of mitochondrial mediated necroptosis triggered by specific extracellular alarmins as the underlying cardiomyocyte cell death pathways, leading to cardiac dysfunction in trauma patients. However, the role of AIF and necroptosis is still poorly understood in the realm of organ injury and unexamined in the context of trauma. Therefore, it is pertinent to conduct further studies to modulate AIF translocation and examine its effect on necroptosis, cell survival and therefore cardiac dysfunction in models prior to translation to humans. Our modeling approach will support further mechanistic studies on the role of inflammatory mediators in driving specific tissue/organ dysfunction after trauma, particularly allowing for the use of transgenic animals for inflammatory pathways.

There are several limitations to this study. We limited our model to 3 h, and longer durations will be required to examine the longer term impacts of injury on cardiac function. The implementation of serial echocardiography to guide resuscitation is unique in trauma models and delivers a new *in-vivo* understanding of cardiac dysfunction in trauma hemorrhage. However, it was difficult to assess myocardial contractility with ultrasound and further advanced imaging approaches such as speckle tracking or MRI tagging could be used to explore this, as well as *ex-vivo* isolated heart techniques. Monitoring of other clinically relevant resuscitation parameters like urine output, arterial blood gas, or central venous pressure could also have been explored, but their implementation in this echo-guided trauma mouse model remain challenging due to low blood volumes and technical limitations. Our inflammatory and biochemical analyses identified cardiomyocyte cell death suggesting, but not definitive of, activation of necroptosis pathways. Further work will be required, to fully characterize the cell death mechanism and its relationship with the sterile inflammatory response.

Cardiac dysfunction is now a major mode of trauma hemorrhage death after admission. We have identified the development of severe and irreversible myocardial damage, despite fluid resuscitation, leading to cardiac dysfunction and death. We pose AIF-driven necroptosis as a possible underlying mechanistic pathway for the cell death. Myocardial protection through novel management strategies and therapeutic approaches represents a major opportunity for improving survival after major trauma.

DATA AVAILABILITY STATEMENT

The datasets generated for this study are available on request to the corresponding author.

ETHICS STATEMENT

This study was carried out in accordance with the recommendations of Home Office guidance on the operation of Animals (Scientific Procedure Act, 1986) in accordance with the EU Directive 2010/63/EU and the Guide for the Care and Use of Laboratory Animals of the National Research Council. The protocols were approved by the Animal Welfare and Ethics Review Board of Queen Mary University of London and conducted under the UK home office license number PC5F29685. Experimental planning and design was performed in accordance with the ARRIVE guidelines for data randomization, blinding for results analysis and sample size calculation. All studies were carried out under non-recovery terminal anesthesia. Animals never regained conscious state, been constantly monitored (MABP, HR, Resp. rate, body temperature) throughout the study. Survival state is defined as the animal's ability to maintain a MAP > 15 mmHg with measurable respiratory and cardiac function. Once any animal reaches any physiological state below the survival threshold, the animals is humanely killed by exsanguination to collect terminal tissue/blood samples.

AUTHOR CONTRIBUTIONS

KB, JW, SN, and JT designed the overall study and experimental programme, together with CT. JW, SN, BP, OB, SM, and JT performed the experiments including animal studies, cell sorting experiments, microscopic studies, and ELISAs. JW, SN, BP, JT, and KB contributed to experimental design and data analysis and coordinated the study and supervised financial support for the

studies. JW, SN, and JT produced initial drafts of the manuscript. CT is the project license holder for the animal work carried out. All authors contributed and revised the drafting of the article and gave final approval of the version to be published.

ACKNOWLEDGMENTS

We acknowledge the support from the Biological Services at QMUL during all the animal studies, from Prof. Adrian Hobbs and his team for their advice on heart IHC and all the members from the Centre for Trauma Sciences for their advice.

SUPPLEMENTARY MATERIAL

The Supplementary Material for this article can be found online at: https://www.frontiersin.org/articles/10.3389/fimmu.2019.02774/full#supplementary-material

REFERENCES

1. Haagsma JA, Graetz N, Bolliger I, Naghavi M, Higashi H, Mullany EC, et al. The global burden of injury: incidence, mortality, disability-adjusted life years and time trends from the Global Burden of Disease study. *Inj Prev*. (2013) 22:3–18. doi: 10.1136/injuryprev-2015-041616
2. Drake SA, Holcomb JB, Yang Y, Thetford C, Myers L, Brock M, et al. Establishing a regional trauma preventable/potentially preventable death rate. *Ann Surg*. (2018) doi: 10.1097/SLA.0000000000002999. [Epub ahead of print].
3. Gunst M, Ghaemmaghami V, Gruszecki A, Urban J, Frankel H, Shafi S. Changing epidemiology of trauma deaths leads to a bimodal distribution. *Proceedings*. (2010) 23:349–54. doi: 10.1080/08998280.2010.11928649
4. Holcomb JB, Jenkins D, Rhee P, Johannigman J, Mahoney P, Mehta S, et al. Damage control resuscitation: directly addressing the early coagulopathy of trauma. *J Trauma*. (2007) 62:307–10. doi: 10.1097/TA.0b013e3180324124
5. Tieu BH, Holcomb JB, Schreiber MA. Coagulopathy: its pathophysiology and treatment in the injured patient. *World J Surg*. (2007) 31:1055–64. doi: 10.1007/s00268-006-0653-9
6. Probst C, Zelle BA, Sittaro NA, Lohse R, Krettek C, Pape HC. Late death after multiple severe trauma: when does it occur and what are the causes? *J Trauma*. (2009) 66:1212–17. doi: 10.1097/TA.0b013e318197b97c
7. Cryer HG, Leong K, McArthur DL, Demetriades D, Bongard FS, Fleming AW, et al. Multiple organ failure: by the time you predict it, it's already there. *J Trauma*. (1999) 46:597–604. doi: 10.1097/00005373-199904000-00007
8. De'Ath HD, Rourke C, davenport R, Manson J, Renfrew I, Uppal R, et al. Clinical and biomarker profile of trauma-induced secondary cardiac injury. *Br J Surg*. (2012) 99:789–97. doi: 10.1002/bjs.8728
9. Naganathar S, De'Ath HD, Wall J, Brohi K. Admission biomarkers of trauma-induced secondary cardiac injury predict adverse cardiac events and are associated with plasma catecholamine levels. *J Trauma Acute Care Surg*. (2015) 79:71–7. doi: 10.1097/TA.0000000000000694
10. Gawande NB, Tumrum NK, Dongre AP. Cardiac changes in hospitalized patients of trauma. *Shock*. (2014) 42:211–17. doi: 10.1097/SHK.0000000000000194
11. Cebelin MS, Hirsch CS. Human stress cardiomyopathy. Myocardial lesions in victims of homicidal assaults without internal injuries. *Hum Pathol*. (1980) 11:123–32. doi: 10.1016/S0046-8177(80)80129-8
12. Fenton KE, Parker MM. Cardiac function and dysfunction in sepsis. *Clin Chest Med*. (2016) 37:289–98. doi: 10.1016/j.ccm.2016.01.014
13. Kalbitz M, Schwarz S, Weber B, Bosch B, Pressmar J, Hoenes FM et al. TREAT Research Group. cardiac depression in pigs after multiple trauma – characterisation of posttraumatic structural and functional alterations. *Sci Rep*. (2017) 7:17861. doi: 10.1038/s41598-017-18088-1
14. Yang S, Zheng R, Hu S, Ma Y, Choudhry MA, Messina JL, et al. Mechanisms of cardiac depression after trauma-hemorrhage: increased cardiomyocyte IL-6 and effect of sex steroids on IL-6 regulation and cardiac function. *Am J Physiol Heart Circ Physiol*. (2006) 287:H2183–91. doi: 10.1152/ajpheart.00624.2003
15. Zhang X, Lu C, Gao M, Cao X, Ha T, Kalbfleisch JH, et al. Toll-like receptor 4 plays a central role in cardiac dysfunction during trauma hemorrhage shock. *Shock*. (2014) 42:31–7. doi: 10.1097/SHK.0000000000000155
16. Zhang X, Gao M, Ha T, Kalbfleisch JH, Williams DL, Li C, Kao RL. The toll-like receptor 9 agonist, CpG-oligodeoxynucleotide 1826, ameliorates cardiac dysfunction after trauma-hemorrhage. *Shock*. (2012) 38:146–52. doi: 10.1097/SHK.0b013e31825ce0de
17. Kilkenny C, Browne WJ, Cuthill IC, Emerson M, Altman DG. Improving bioscience research reporting: the ARRIVE guidelines for reporting animal research. *PLoS Biol*. (2010) 8:e1000412. doi: 10.1371/journal.pbio.1000412
18. Mahler M, Berard M, Feinstein R, Gallagher A, Illgen-Wilcke B, Pritchett-Corning K, et al. FELASA recommendations for the health monitoring of mouse, rat, hamster, guinea pig and rabbit colonies in breeding and experimental units. Working party report. *Lab Anim*. (2014) 48:178–92. doi: 10.1177/0023677213516312
19. Varga T, Mounier R, Patsalos A, Gogolák P, Peloquin M, Horvath A, et al. Macrophage PPARγ, a lipid activated transcription factor controls the growth factor GDF3 and skeletal muscle regeneration. *Immunity*. (2016) 45:1038–51. doi: 10.1016/j.immuni.2016.10.016
20. McArthur S, Gobbetti T, Gaëtan J, Desgeorges T, Theret M, Gondin J, et al. Annexin A1 drives macrophage skewing towards a resolving phenotype to accelerate the regeneration of muscle injury through AMPK activation. *BioRxiv*. (2018) 375709. doi: 10.1101/375709
21. Wall J, Tremoleda J, Brohi K. Heart Fatty Acid Binding Protein (H-FABP) is a biomarker of trauma-induced secondary cardiac injury in a pre-clinical model of trauma-haemorrhage. *Shock*. (2015) 44:21–2. doi: 10.1097/01.shk.0000472071.00900.4e
22. Montazer SH, Jahanian F, Khatir IG, Bozorgi F, Assadi T, Pashaei SM, et al. Prognostic value of cardiac troponin I and T on admission in mortality of multiple trauma patients admitted to the emergency department: a prospective follow-up study. *Med Arch*. (2019) 73:11–14. doi: 10.5455/medarh.2019.73.11-14
23. Bland RD, Shoemaker WC, Abraham E, Cobo JC. Hemodynamic and oxygen transport patterns in surviving and nonsurviving postoperative patients. *Crit Care Med*. (1985) 13:85–90. doi: 10.1097/00003246-198502000-00006
24. Sauaia A, Moore FA, Moore EE, Moser KS, Brennan R, Read RA, et al. Epidemiology of trauma deaths: a reassessment. *J Trauma*. (1995) 38:185–19. doi: 10.1097/00005373-199502000-00006
25. Frencken JF, Donker DW, Spitoni C, Koster-Brouwer ME, Soliman IW, Ong DSY, et al. Myocardial injury in patients with sepsis and its association with long-term outcome. *Circ Cardiovasc Qual Outcomes*. (2018) 11:e004040. doi: 10.1161/CIRCOUTCOMES.117.004040
26. De'Ath H, Manson J, Davenport R, Glasgow S, Renfrew I, Davies L, et al. Trauma-induced secondary cardiac injury is associated with hyperacute elevations in inflammatory cytokines. *Shock*. (2013) 39:415–20. doi: 10.1097/SHK.0b013e31828ded41
27. Swirski FK, Nahrendorf M, Etzrodt M, Wildgruber M, Cortez-Retamozo V, Panizzi P, et al. Identification of splenic reservoir monocytes and their deployment to inflammatory sites. *Science*. (2009) 325:612–6. doi: 10.1126/science.1175202
28. Liu J, Wang H, Li J. Inflammation and inflammatory cells in myocardial infarction and reperfusion injury: a double-edged sword. *Clin Med Insights Cardiol*. (2016) 10:79–84. doi: 10.4137/CMC.S33164
29. Feng Y, Liu Y, Wang D, Zhang X, Liu W, Fu F, et al. Insulin alleviates post trauma cardiac dysfunction by inhibiting tumor necrosis factor-alpha-mediated reactive oxygen species production. *Crit Care Med*. (2013) 41:e74–84. doi: 10.1097/CCM.0b013e318278b6e7
30. Tummers B, Green DR. Caspase-8: regulating life and death. *Immunol Rev*. (2017) 277:76–89. doi: 10.1111/imr.12541
31. Baritaud M, Cabon L, Delavallée L, Galán-Malo P, Gilles ME, Brunelle-Navas MN, et al. AIF-mediated caspase-independent necroptosis requires ATM and

DNA-PK-induced histone H2AX Ser139 phosphorylation. *Cell Death Dis.* (2012) 3:e390. doi: 10.1038/cddis.2012.120
32. Davidovich P, Kearney CJ, Martin SJ. Inflammatory outcomes of apoptosis, necrosis and necroptosis. *Biol Chem.* (2014) 395:1163–71. doi: 10.1515/hsz-2014-0164
33. Wang G, Qu FZ, Li L, Lv JC, Sun B. Necroptosis: a potential, promising target and switch in acute pancreatitis. *Apoptosis.* (2016) 21:121–9. doi: 10.1007/s10495-015-1192-3
34. Zhao H, Jaffer T, Eguchi S, Wang Z, Linkermann A, Ma D. Role of necroptosis in the pathogenesis of solid organ injury. *Cell Death Dis.* (2015) 6:e1975. doi: 10.1038/cddis.2015.316

Conflict of Interest: The authors declare that the research was conducted in the absence of any commercial or financial relationships that could be construed as a potential conflict of interest.